Phase transformation induced by irradiating an $Al_{62}Cu_{25.5}Fe_{12.5}$ icosahedral quasicrystal

1995 J. Phys.: Condens. Matter 7 2105

(http://iopscience.iop.org/0953-8984/7/10/017)

J. Phys.: Condens. Matter 7 (1995) 2105–2114. Printed in the UK

Phase transformation induced by irradiating an $Al_{62}Cu_{25.5}Fe_{12.5}$ icosahedral quasicrystal

Renhui Wang†, Xiangxiu Yang†, Heishichiro Takahashi‡ and Somei Ohnuki‡

† Department of Physics, Wuhan University, 430072 Wuhan, People's Republic of China
‡ Metal Research Institute, Faculty of Engineering, Hokkaido University, Sapporo 060, Japan

Received 6 October 1994

Abstract. The irradiation effect of the $Al_{62}Cu_{25.5}Fe_{12.5}$ icosahedral quasicrystal (IQC) induced by 120 keV Ar ions and 1 MeV electrons has been studied *in situ* using high-voltage electron microscope–ion accelerator dual-irradiation facilities. The effect is dose and temperature dependent and we can define three critical temperatures T_c, T_d and T_p. When irradiated at $T < T_c$, the IQC is transformed into a crystalline microtwin oriented according to icosahedral symmetry. When $T > T_c$, the IQC remains an IQC but with a higher (when $T > T_d$) or lower (when $T < T_d$) degree of perfection. The planar defects originally existing in the $Al_{62}Cu_{25.5}Fe_{12.5}$ IQC foils are stable when $T > T_p$ but disappear when $T < T_p$. For the $Al_{62}Cu_{25.5}Fe_{12.5}$ IQC, we found that $T_c \simeq 400$ K, $T_d \simeq 450$ K (for 1 MeV electrons) or 550 K (for 120 keV Ar ions) and $T_p \simeq 600$ K.

1. Introduction

Irradiation-induced phase transformation in crystals has been an interesting research field for the past 20 years [1]. Since the discovery of icosahedral quasicrystals (IQCs) in Al-based alloys by Shechtman *et al* [2], there have been some papers studying irradiation-induced phase transformation in IQCs. Urban *et al* [3] and Mayer *et al* [4] irradiated Al–Mn and Al–V IQCs by 1 MeV electrons. They found that IQCs were transformed into an amorphous phase when the irradiation temperature was sufficiently low and observed a reverse transition by post-irradiation heating. Wang *et al* [5] and Wang *et al* [6] studied phase transformations in an $Al_{76}Si_4Mn_{20}$ IQC induced by 120 keV Ar^+ ions and/or 1 MeV electrons. They found an amorphization effect when irradiated at lower temperatures (345 K or less for Ar ions; room temperature (RT) or less for electrons) and a disordering effect at medium temperatures. Under special irradiation conditions an $Al_{76}Si_4Mn_{20}$ simple IQC may be transformed into an ordered face-centred IQC [5]. Recently, Wang *et al* [7] irradiated an $Al_{62}Cu_{25.5}Fe_{12.5}$ IQC at RT with 120 keV Ar ions and observed an irradiation-induced phase transformation from an IQC to a CsCl(B2)-based structure and a reverse transition during heating.

The high-voltage electron microscope–ion accelerator dual-irradiation facilities installed at Hokkaido University [8] and equipped with a double-tilting heating stage provided a powerful tool for *in situ* observation of the temperature-dependent ion and/or electron irradiation effect. By using this facility we have studied phase transformations in an $Al_{62}Cu_{25.5}Fe_{12.5}$ IQC induced by irradiation of 1 MeV electrons and 120 keV Ar ions to different doses at different temperatures, and new results are reported.

0953-8984/95/102105+10$19.50

2. Specimen preparation and experimental method

The alloy of composition $Al_{62}Cu_{25.5}Fe_{12.5}$ was prepared by melting the high-purity elements in an induction furnace under an Ar atmosphere. The ingot was annealed at 1095 K for 47.2 h, cooled for 30 h to RT and then cut into slices of 3 mm in diameter. A synchrotron radiation topography study [9] showed that these slices are perfect IQCs with very large grains ranging from 0.1 to 3 mm in diameter. Foils for transmission electron microscopy (TEM) were prepared by mechanical thinning and Ar^+ ion milling.

The Hitachi H-1300 high-voltage electron microscope–ion accelerator dual-irradiation facilities equipped with a double-tilting heating stage were used to heat and irradiate the TEM specimens at a given temperature. The high-energy particles utilized in the present work were 1 MeV electrons and/or 120 keV Ar ions. The electron beam current in the small irradiated region of 1 μm diameter was 9.4 A cm^{-2} and the argon ion beam current covering the whole TEM specimen was unstable, ranging from 0.3 to 0.6 μA cm^{-2}.

The contrast images and electron diffraction patterns (EDPs) of the specimens were observed *in situ* by the Hitachi H-1300 high-voltage electron microscope operated at 1 MeV. A theoretical calculation shows that the projected range is 74.8 nm with 29.6 nm longitudinal straggling and 30.0 nm lateral straggling when the $Al_{62}Cu_{25.5}Fe_{12.5}$ alloy is bombarded by 120 keV Ar^+ ions, which is comparable with the foil thickness of the thin regions. For thicker regions observable by 1 MeV electrons in the high-voltage electron microscope, only the top surface layer of the foil was bombarded by the ions. On the other hand, most of the irradiated 1 MeV electrons were transmitted through the observable regions of the specimen.

3. Results

3.1. Microstructure and electron diffraction patterns before irradiation

TEM observation showed that the $Al_{62}Cu_{25.5}Fe_{12.5}$ foils before irradiation are all face-centred IQCs, of which the EDPs along the fivefold (A5), twofold (A2), threefold (A3) and pseudo-twofold (A2P) axes are shown in figures 1(a), 1(b), 1(c) and (d), respectively. The grain is so large that the whole thin region of a foil belongs to a single grain, in accordance with the synchrotron radiation white-beam topography observation [9]. These foils contain high-density planar defects which appear as straight fringes parallel to the intersection lines of these planar defects with the foil surface, as shown in figure 1(e) which was photographed when one A5 axes of this grain is parallel to the incident beam, as studied already by Yang *et al* [10].

3.2. Simulated electron diffraction patterns of the CsCl-type microcrystals arranged according to the icosahedral symmetry

Figures 2(a), 2(b), 2(c) and 2(d) are EDPs after the $Al_{62}Cu_{25.5}Fe_{12.5}$ TEM foils have been irradiated with 120 keV Ar ions, along the original A5, A2, A3 and A2P axes of the IQC, corresponding to figures 1(a), 1(b), 1(c) and 1(d), respectively. These EDPs still show fivefold, twofold, threefold and pseudo-twofold symmetries respectively but are quite different compared with figures 1(a), 1(b), 1(c) and 1(d). Some spots, such as A, B, C and D (in figure 2), are very strong compared with the corresponding spots in fiugre 1 while others, such as E, F and G (in figure 2), are very broad along the tangential direction and form arc sections. Most of the weak spots in figure 1 disappear in figure 2 and some spots

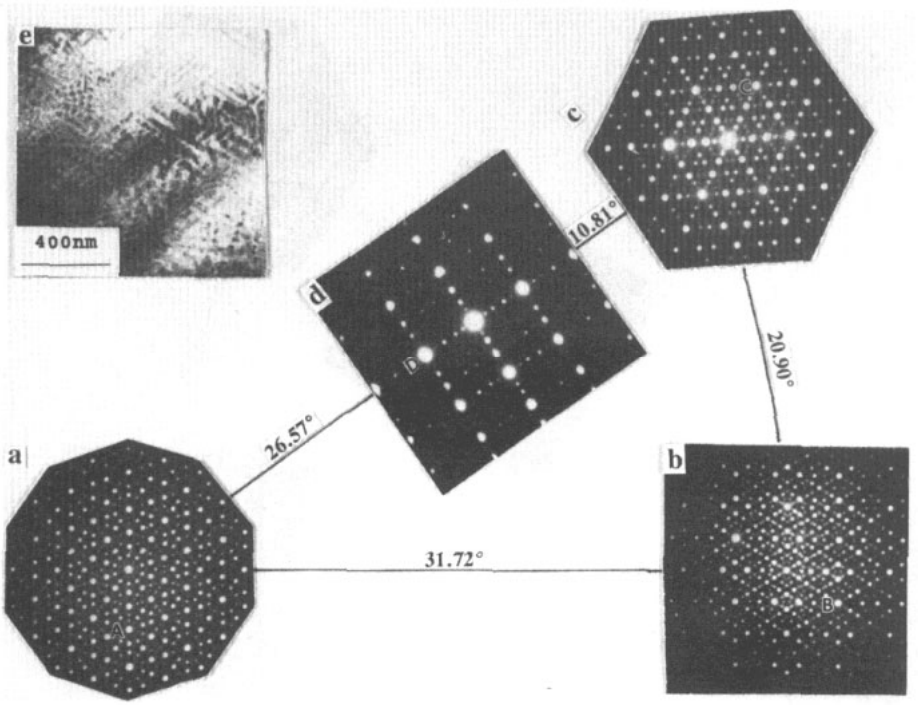

Figure 1. (a)–(d) EDPs along the (a) A5, (b) A2, (c) A3 and (d) A2P zone axes and (e) a BF image of the $Al_{62}Cu_{25.5}Fe_{12.5}$ IQC before irradiation.

such as G and H (in figure 2) do not exist in figure 1. In addition, after Ar ion irradiation, the straight-line contrast pertaining to the planar defects shown in figure 1(e) disappears and divides into dark speckles of size ranging from 10 to 70 nm in the bright-field (BF) image as shown in figure 2(e).

The irradiation-induced phase and its microstructure, as shown in figure 2, may be identified as follows: as pointed out by Wang *et al* [7], 120 keV Ar^+ ion irradiation induces the $Al_{62}Cu_{25.5}Fe_{12.5}$ IQC to transform to a CsCl(B2)-type phase with the following orientational relationship:

$$A(5)(\text{IQC}) \parallel [110](B2)$$

$$A2(\text{IQC}) \parallel [11\bar{1}](B2).$$

If the B2-type phase has very small grains, then it is reasonable to suppose that these grains form microtwins oriented according to the icosahedral symmetry. On the basis of this supposition, EDPs of the icosahedral microtwins of B2-type phase have been simulated as shown in figure 3, where the double-reflection effect has been considered. For example, the spot O in figure 3(a) is a double reflection contributed by reflections P and R. Moreover, considering the possible broadening effect of the reciprocal point, the curving effect of the TEM foils and the small divergence of the incident beam, we have supposed that, when a reciprocal vector is nearly perpendicular to the zone axis within a given error range of 0.8°, this reciprocal point may contribute to this zone-axis EDP if it possesses a sufficiently high intensity. Comparing figures 3(a), 3(b), 3(c) and 3(d) with figures 2(a), 2(b), 2(c) and 2(d) we find very good agreement, which indicates that the Ar-ion-induced B2-type phase is arranged as icosahedral microtwins.

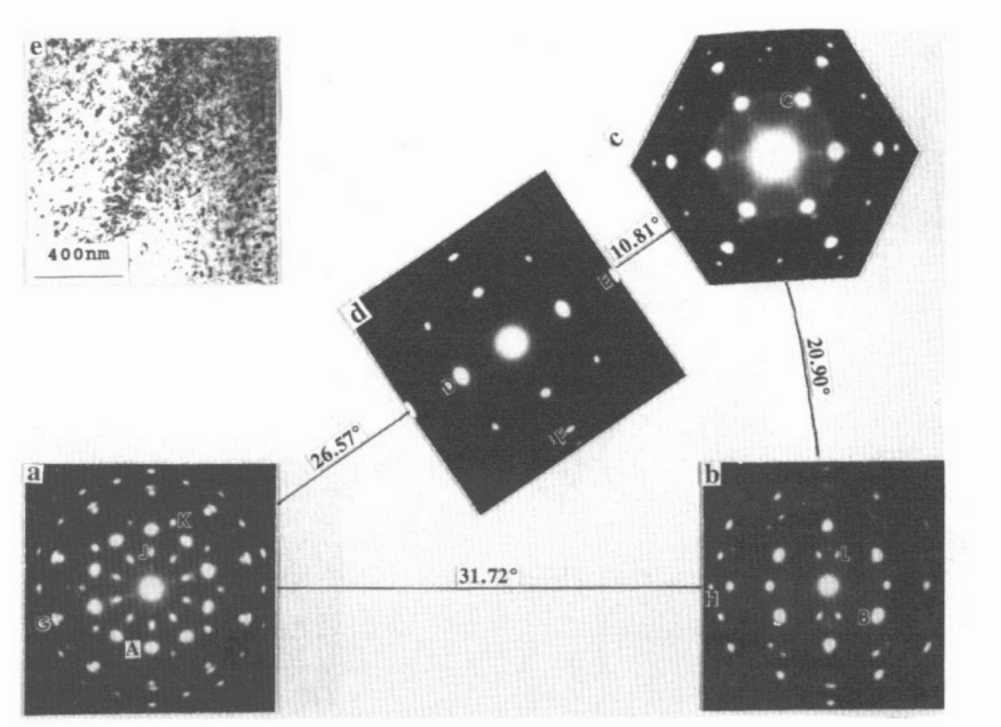

Figure 2. (a)–(d) EDPs along the original icosahedral (a) A5, (b) A2, (c) A3 and (d) A2P zone axes and (e) a BF image of the Al–Cu–Fe foil after 120 keV Ar ion irradiation.

3.3. 1 MeV electron irradiation effect

We have studied the 1 MeV electron irradiation effect at different temperatures (RT to 890 K) and different doses (up to 3.2×10^{23} e^- cm^{-2}) by *in situ* observation of the EDPs and contrast images. At RT the irradiation effect is discernible when the dose reaches about 2×10^{22} e^- cm^{-2}. The straight contrast breaks up and some speckle contrast appears. At the same time, the differences between the intensities of the reflection spots in the EDPs increases and some strong spots broaden along the tangential direction. With increasing electron dose, the EDPs and contrast images become similar to those shown in figure 2. Figures 4(a) and 4(b) compare the EDPs along the A2(IQC) zone axis and figures 4(c) and (d) along the A5(IQC) zone axis; the BF images are shown in figures 4(e) and 4(f). Figures 4(a), 4(c) and 4(e) were obtained before and figures 4(b), 4(d) and 4(f) after 1 MeV electron irradiations to a dose of 3.2×10^{23} e^- cm^{-2} at RT. Thus it can be concluded that the $Al_{62}Cu_{25.5}Fe_{12.5}$ IQC is transformed into microtwins of B2-type phase oriented according to icosahedral symmetry.

The electron irradiation effect is also temperature dependent. At lower temperatures (290–360 K), the effect is the same as at RT, i.e. the IQC phase is transformed into icosahedral microtwins of B2-type phase, as shown in figures 5(g) and 5(h) (irradiated at 360 K to a dose of 1.1×10^{23} e^- cm^{-2}) compared with figures 5(a) and 5(b) photographed before irradiation. At higher temperatures (470–890 K), EDPs still correspond to those of a face-centred IQC with better perfection; compare figure 5(b) with figure 5(d), where figure 5(d) (at 470 K) shows additional spots with weaker intensity than figure 5(b) does. When the temperature is very high (710–890 K), no change in BF images can be observed. At medium temperatures (420–580 K), the planar defects are broken up partly; compare figure 5(c) (irradiated at 470 K) and figure 5(e) (at 420 K) with figure 5(a). When irradiated at 420 K, the EDPs

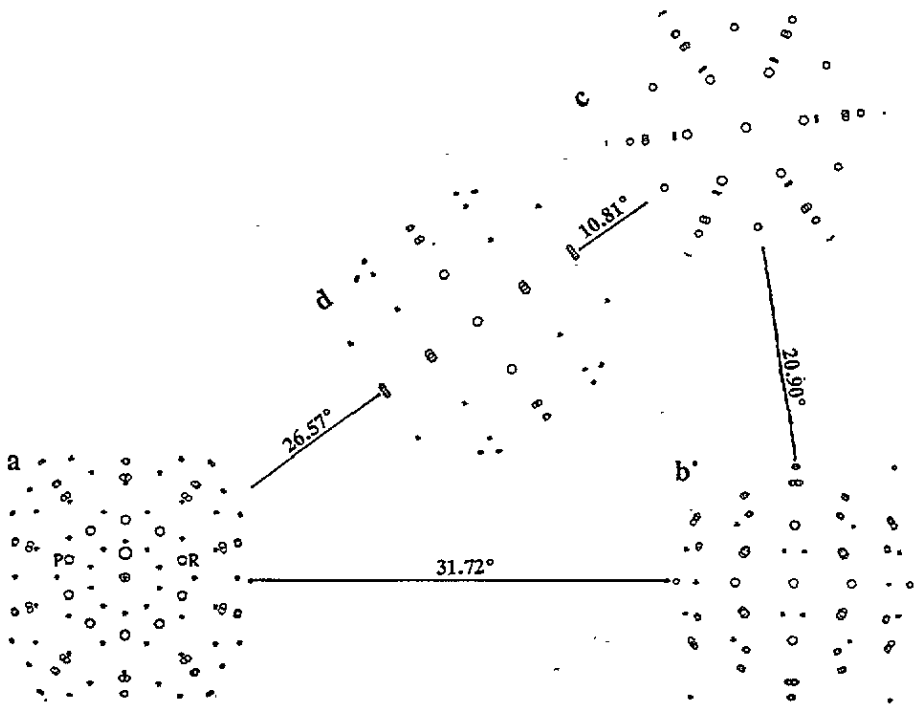

Figure 3. Simulated EDPs along the original icosahedral (a) A5, (b) A2, (c) A3 and (d) A2P zone axes of crystalline microtwins of B2-type phase arranged according to the icosahedral symmetry.

still correspond to an IQC (figure 5(f)) but with lower perfection compared with that before irradiation (figure 5(b)).

3.4. Heating experiment after electron irradiation

The electron-irradiated TEM foil (at RT) was heated in the high-voltage electron microscope and observed *in situ*. When the temperature was lower than 810 K; no discernible change in the BF images and EDPs of the foil was observed. When the foil was heated to 855 K, some larger grains about 0.1 μm in size appeared and these eventually grew to yield a polycrystalline aggregate of B2-type grains (about 0.5 μm in mean diameter) when the heating time was increased to 30 min. These large grains maintained their sizes, shapes and orientations after the foil had been cooled to RT. Figure 6 shows an example of the foil which was irradiated by 1 MeV electrons at RT to a dose of 3.2×10^{23} e^- cm^{-2}, heated at 855 K for 30 min and then cooled to RT. Figures 6(a) and (c) show dark-field (DF) images by selecting reflections B1 (figure 6(b)) and C1 (figure 6(d)), respectively, where the reflection B1 belongs to the EDP of the $[113]_B$ (B2) zone axis and the reflection C1 belongs to the EDP of the $[113]_C$ (B2) zone axis. The fact that grain B in figure 6(a) and grain C in figure 6(c) are bright indicates that the EDPs $[113]_B$ and $[113]_C$ are produced by grains B and C, respectively. This indicates that grains B and C are related by a fivefold rotation around the A5(IQC) axis.

For the foil irradiated by 1 MeV electrons at 360 K to a dose of 1.1×10^{23} e^- cm^{-2}, which was transformed into icosahedral microtwins of B2 phase (figures 5(g) and 5(h)), no change was observed when the heating temperature was lower than 690 K. After the

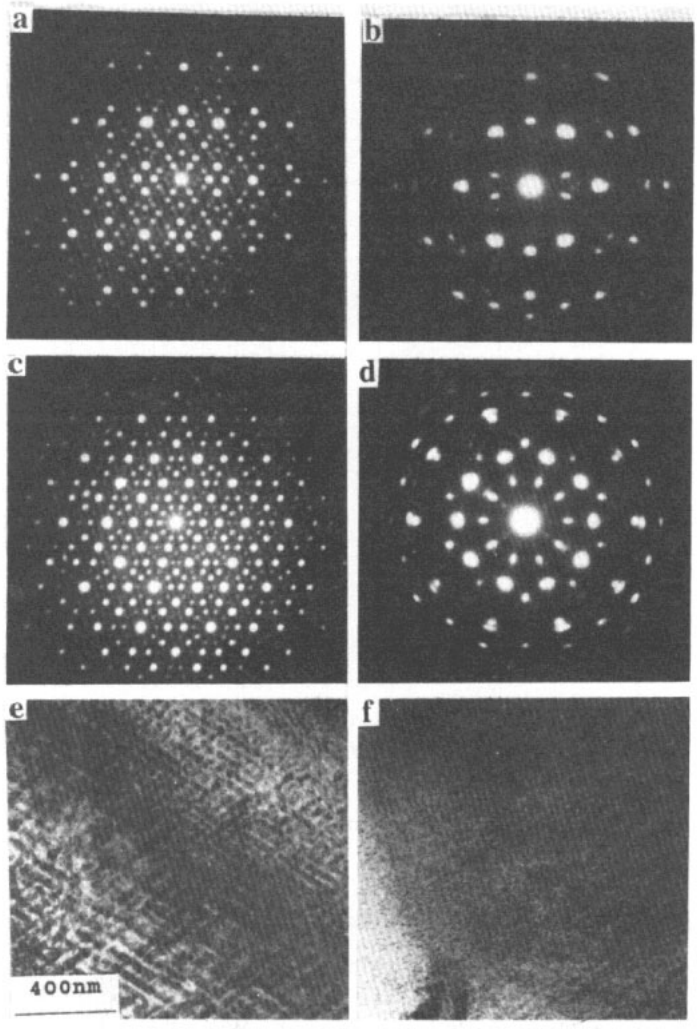

Figure 4. (a)–(d) EDPs along (a), (b) A2 and (c), (d) A5 zone axes and (e), (f) BF images of the $Al_{62}Cu_{25.5}Fe_{12.5}$ foil (a), (c), (e) before and (b), (d), (f) after 1 MeV electron irradiation (to a dose of 3.2×10^{23} e^- cm^{-2} at RT).

specimen had been annealed at 820 K for more than 45 min, the EDP changed from the microtwin type (figure 5(h)) to the IQC type, similar to figure 5(f) but less perfect.

3.5. 120 keV Ar ion irradiation effect

Since the whole foil is irradiated with Ar ions, experiments observing the temperature-dependent ion irradiation effect were arranged as follows. Firstly a foil was heated to a high temperature (about 810 K) and the Ar ion irradiation effect was observed until a given dose (about 2×10^{15} Ar^+ cm^{-2}) was reached. Then the temperature was lowered stepwise and observation of the irradiation effect was repeated. The experiments showed that there was no discernible change when the irradiation temperature was higher than

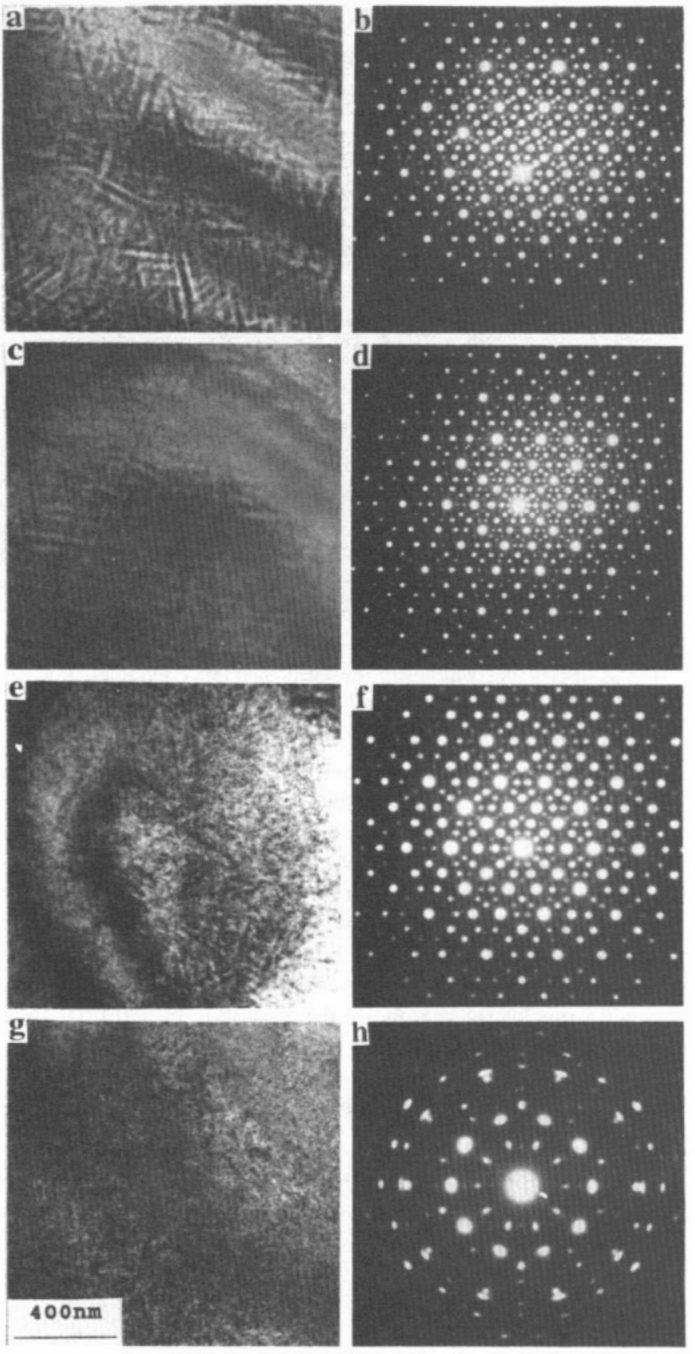

Figure 5. (b), (d), (f), (h) EDPS along the A5 zone axis and (a), (c), (e), (g) BF images of the $Al_{62}Cu_{25.5}Fe_{12.5}$ foils (a), (b) before and (c)–(h) after 1 MeV electron irradiating at (c), (d) 470 K, (e), (f) 420 K and (g), (h) 360 K to a dose of 1.1×10^{23} e^{-} cm^{-2}.

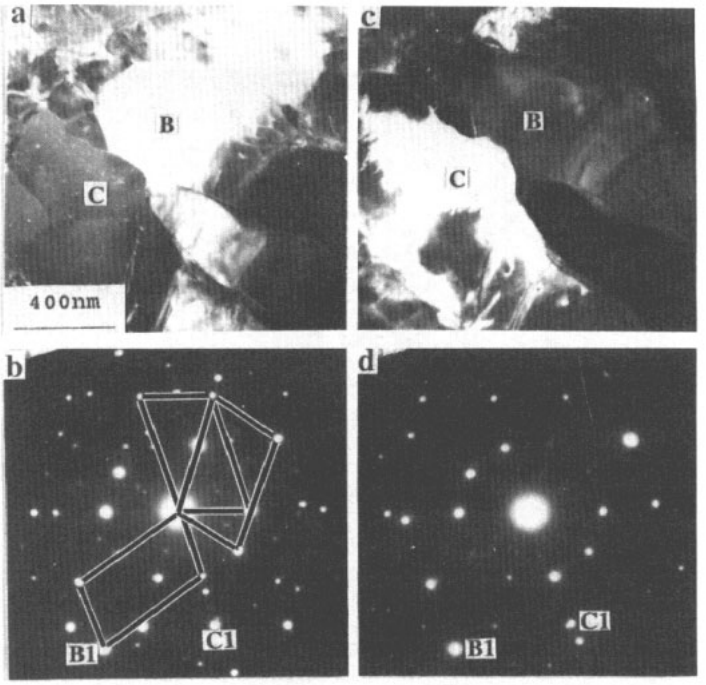

Figure 6. (a), (c) DF images and (b), (d) EDPs along the original A5 (IQC) axis of the $Al_{62}Cu_{25.5}Fe_{12.5}$ foil which was irradiated by 1 MeV electrons at RT to a dose of 3.2×10^{23} e^- cm^{-2}, heated at 855 K for 30 min and then cooled to RT.

600 K. When the temperature was lowered to 400 K, the EDP (figure 7(f)) was characteristic of icosahedral microtwins of the B2-type phase and the BF image (figure 7(e)) assumed a speckle contrast. The EDPs along other zone axes such as A5(IQC), A3(IQC) and A2P(IQC) from the specimens irradiated with 120 keV Ar ions at a temperature lower than 400 K show similar characteristics (figure 2). After irradiation at a medium temperature (500 K) to a dose of 2×10^{15} or 4×10^{15} Ar^+ cm^{-2}, the IQC partly transformed into B2-type microtwins and the remaining IQC structure became less perfect, as shown in figure 7(d). The latter consists of EDPs of both a B2-type microtwin (cf figure 7(f)) and an IQC (similar to figure 7(b) but with much less sharpness of the spots). In addition, the straight fringes pertaining to the planar defects (figure 7(a)) become broken (figure 7(c)).

3.6. Electron and Ar ion dual-irradiation effect

During Ar ion irradiation we also converged the incident electron beam to irradiate a small region of 1 μm diameter. In this way both the ion irradiation (without electron irradiation) and the ion and electron dual-irradiation experiments were carried out simultaneously. The experiment shows that the dual irradiation gives the same effect as Ar ion irradiation alone.

4. Discussion

From the experimental results described in section 3 it is evident that there exist three critical temperatures T_c, T_d and T_p. At lower temperatures ($T < T_c$) the IQC is transformed

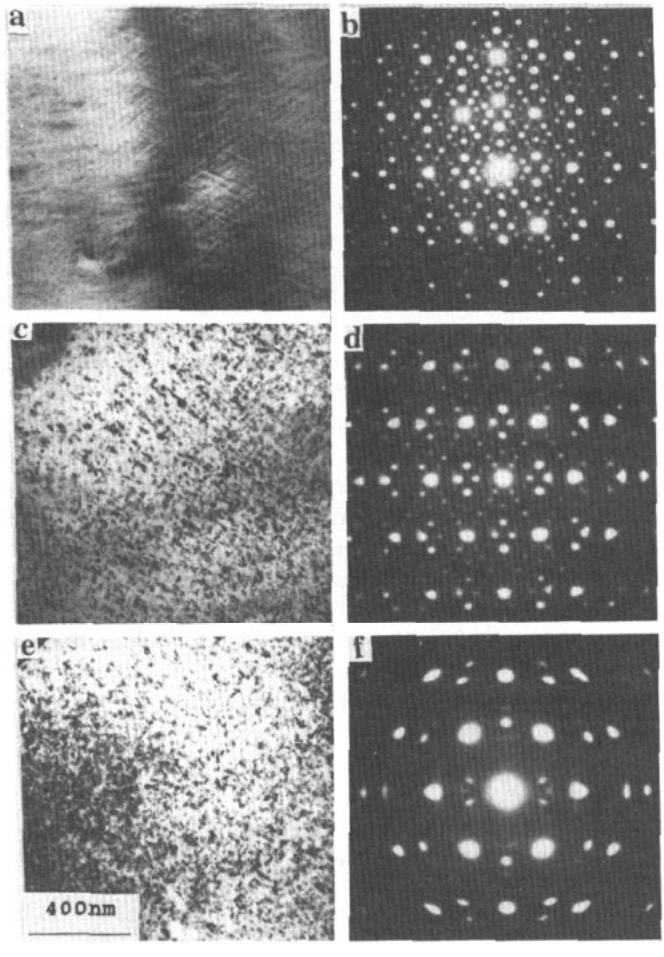

Figure 7. (a), (c), (e) BF images and (b), (d), (f) EDPS along original A2(IQC) axis of the $Al_{62}Cu_{25.5}Fe_{12.5}$ *foils* (a), (b) before and (c)–(f) after 120 keV Ar ion irradiation (c), (d) at 500 K to a dose of 4×10^{15} Ar^+ cm^{-2} and (e), (f) at 400 K to a dose of 2×10^{15} Ar^+ cm^{-2}.

into crystalline microtwins oriented according to the icosahedral symmetry. At very high temperatures ($T > T_p$), the face-centred IQC phase with planar defects persists and the degree of perfection of the IQC may increase. When $T_d < T < T_p$, the degree of perfection of the IQC increases but the planar defects disappear. At medium temperatures ($T_c < T < T_d$), the specimen structure remains an IQC but with lower degree of perfection. For the $Al_{62}Cu_{25.5}Fe_{12.5}$ IQC, we found that $T_c \simeq 400$ K, $T_d \simeq 450$ K (for 1 MeV electrons) or 550 K (for 120 keV Ar ions) and $T_p \simeq 600$ K.

According to the phase diagram of the ternary Al–Cu–Fe system [11], $Al_{62}Cu_{25.5}Fe_{12.5}$ is a stable IQC in the temperature range higher than 673 K. Wang *et al* [7] found that an enhanced diffusion rate induced by Ar^+ irradiation accelerated the transformation from the $Al_{62}Cu_{25.5}Fe_{12.5}$ IQC to a B2-type phase at RT. By considering this and the competition between the damage rate and the recovery rate caused by radiation-induced diffusion and thermal annealing (which is dependent on temperature), one can explain the temperature-

dependent irradiation effect as follows: at higher temperatures ($T > T_d$), the recovery process dominates, and hence no damage can be found; rather the thermal and irradiation-enhanced diffusion may increase the degree of order of the IQC. When the temperature is lower than the IQC $\rightarrow$ B2-phase transformation point, irradiation-enhanced diffusion may accelerate this transformation. At medium temperatures ($T_c < T < T_d$), at the beginning of the irradiation, the recovery process is slower than the damage accumulation process which induces a decrease in the degree of order (or of the perfection) of the IQC. On increase in the defect density, defect-enhanced diffusion accelerates the recovery process until a dynamic balance is reached between the recovery and damage processes. Moreover, one can suppose that the planar defects are metastable at temperatures lower than T_p and hence that irradiation-enhanced diffusion accelerates the disappearance of the planar defects when $T < T_p$.

There is a substantial difference between the behaviour of Al–Cu–Fe IQC on the one hand and the Al–Mn [3], Al–V [4] and Al–Si–Mn [6] IQCs on the other hand after low-temperature irradiation. The former is transformed into a stable crystalline phase and the latter are transformed into the amorphous state. This may be explained by the higher degree of imperfection in the rapidly solidified Al–Mn, Al–V and Al–Si–Mn IQCs and the intimate structural relationship between the Al–Cu–Fe face-centred IQC and B2-type phases.

It shall be noted that both the microtwin structure (cf section 3.4 of the present paper) and the large grains (cf [7]) of the B2-type phase transformed from the IQC phase by irraadiation can reversibly transform to the IQC phase after heating to 820 K (cf section 3.4) or 880 K [7] under certain conditions. This supports the conclusion that the $Al_{62}Cu_{25.5}Fe_{12.5}$ IQC phase is stable at higher temperatures and metastable at RT. The transformation temperature may be nearly equal to the temperature T_c ($\simeq$ 400 K) as revealed by the present study.

Acknowledgment

This project was supported by the National Natural Science Foundation of China.

References

[1] Nolfi F V 1983 *Phase Transformations During Irradiation* (London: Applied Science)
[2] Shechtman D, Blech I, Gratias D and Cahn J W 1984 *Phys. Rev. Lett.* **53** 1951
[3] Urban K, Moser N and Kronmüller H 1985 *Phys. Status Solidi* a **91** 411
[4] Mayer J, Urban K and Fidler J 1987 *Phys. Status Solidi* a **99** 467
[5] Wang Z G, Deng W F and Wang R 1992 *Phys. Status Solidi* a **133** 299
[6] Wang R, Takahashi H, Ohnuki S and Wang Z G 1994 *Radiat. Eff. Defects Solids* **129** 173
[7] Wang Z G, Yang X X and Wang R 1993 *J. Phys.: Condens. Matter* **5** 7569
[8] Takeyama T, Ohnuki S and Takahashi H 1985 *J. Nucl. Mater.* **133–4** 571
[9] Zou W H, Wang R, Gui J, Zhao J Y and Jiang J H 1994 *J. Appl. Crystallogr.* **27** 13
[10] Yang X X, Wang Z G and Wang R 1994 *Phil. Mag. Lett.* **69** 15
[11] Gratias D, Calvayrac Y, Devaud-Rzepski J, Faudot F, Harmelin M, Quivy A and Bancel P A 1993 *J. Non-Cryst. Solids* **153–4** 482